

Response to Comments on the Manuscript (essd-2023-28):

Seamless mapping of long-term (2010-2020) daily global XCO₂ and XCH₄ from GOSAT, OCO-2, and CAMS-EGG4 with a spatiotemporally self-supervised fusion method

Dear Editors and Referees,

We would like to sincerely express our gratitude to you for your careful reading and constructive comments.

According to the comments, we have tried our best to improve the manuscript, and an item-by-item response follows. The modified parts have been highlighted in yellow color in the revised manuscript.

Once again, we are particularly grateful for your careful reading and constructive comments. Thanks very much for your time.

Best regards,

Qiangqiang Yuan

Response to Comments of Referee #1:

General comments:

The manuscript designed a self-supervised fusion method based on spatiotemporal Discrete Cosine Transform to fuse sparse satellite data and global full-coverage GHGs reanalysis data for the seamless estimation of long-term daily global XCO₂ and XCH₄. It is an interesting study, especially for providing long-term XCO₂ and XCH₄ datasets that don't need any auxiliary variables and analyzing the global pattern of XCO₂ and XCH₄ trends. I think the paper needs minor revision before acceptance for publication.

Response: We would like to take this opportunity to gratefully thank the referee for his/her comments and recommendations for improving the paper. An item-by-item response to the constructive comments follows. Thanks for your time.

Specific comments:

Q1.1: The assessments of spatial distribution on a daily temporal scale may be necessary for a daily dataset.

Response: Thank the referee for his/her valuable comment. The assessments of spatial distribution on a daily temporal scale have been appended in the manuscript.

The main revision is as follows:

Figure 12 illustrates the examples of daily fused XCO₂ and XCH₄ over the globe, consisting of three days in three years. As shown, the fused results display detailed information on atmospheric CO₂ and CH₄, which clearly indicate their regional and global spatial patterns. In addition, incoherent or factitious spatial distribution is not observed in the fused XCO₂ and XCH₄. Next, Fig. 13 provides the corresponding daily XCO₂ and XCH₄ from GOSAT and OCO-2 over the globe. It is worth noting that the daily satellite XCO₂ and XCH₄ are mapped via footprints due to their significant sparse coverage, which are nearly invisible at grids of 0.25°. As expected, the fused results present identical spatial distribution compared to XCO₂ and XCH₄ from GOSAT and OCO-2. This suggests the robustness and reliability of the proposed fusion method.

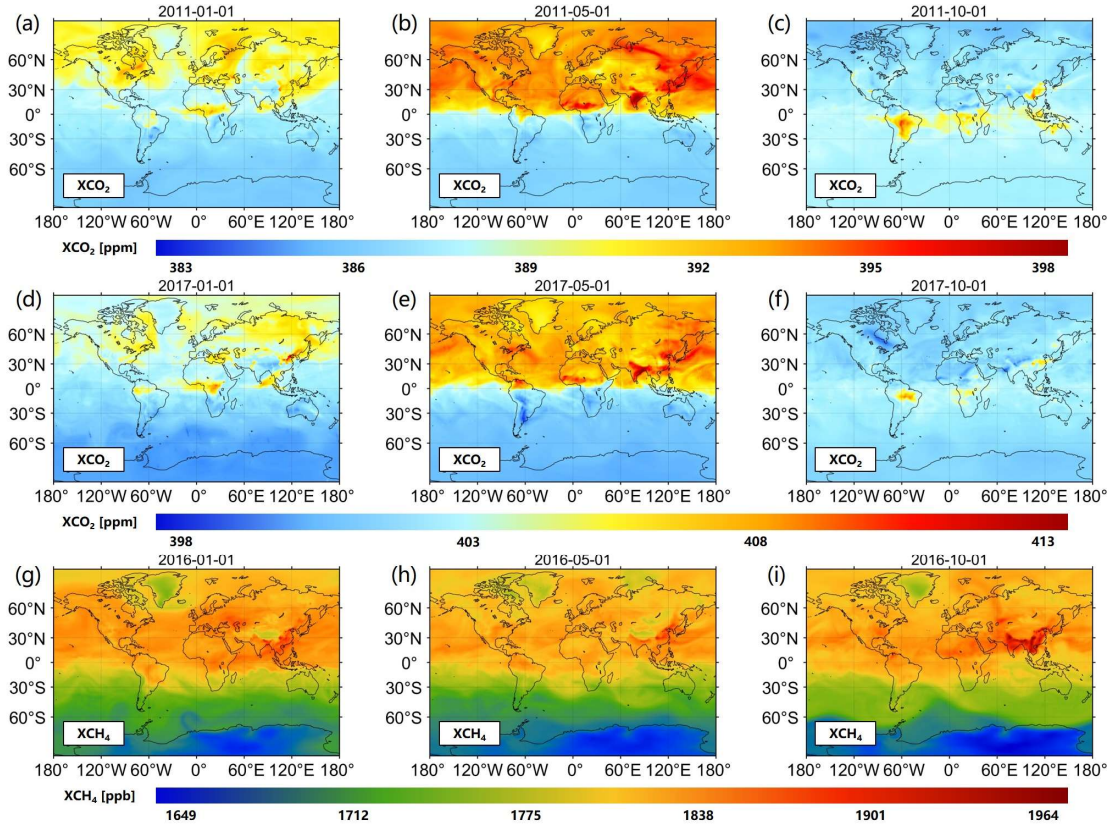


Figure 12. Daily fused (a-f) XCO₂ and (g-i) XCH₄ over the globe. Color ramps stand for the values of XCO₂ and XCH₄.

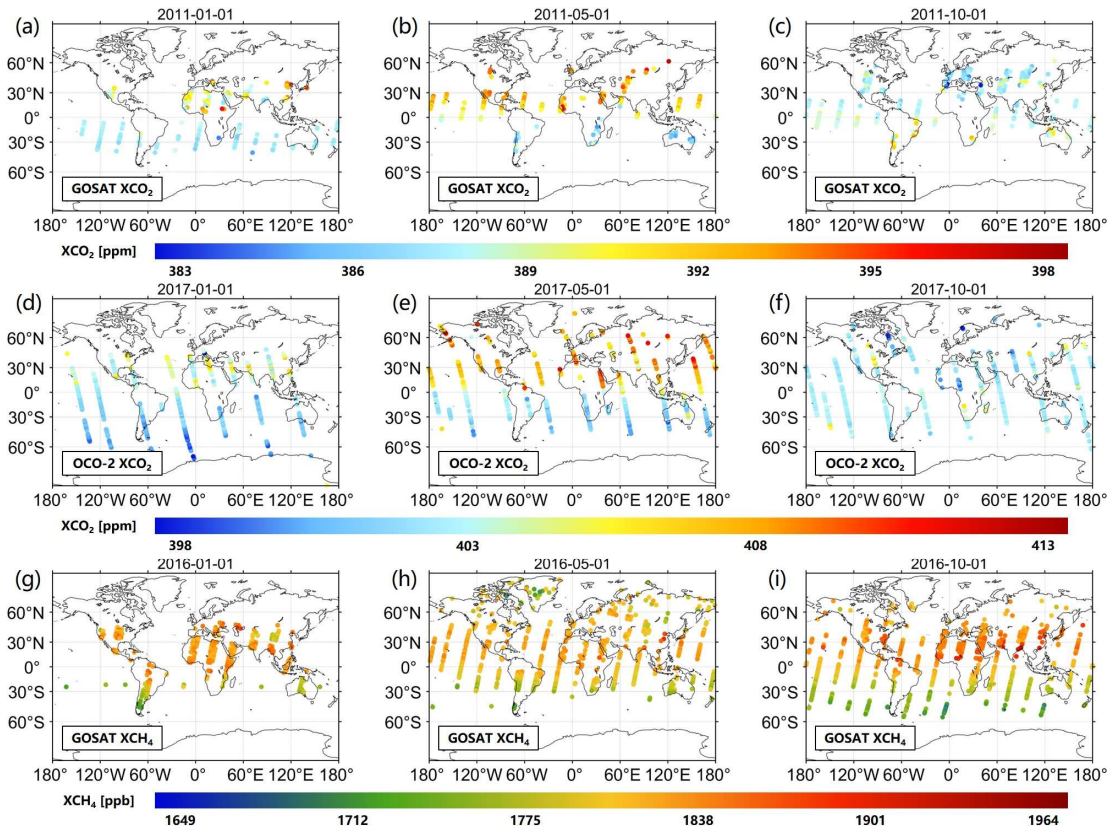


Figure 13. Daily (a-c) GOSAT, (d-f) OCO-2 XCO₂, and (g-i) GOSAT XCH₄ over the globe. Color ramps stand for the values of XCO₂ and XCH₄.

Q1.2: Satellite XCO₂ of 2010-2014 and 2015-2020 come from two datasets. It is crucial for users who rely on the long-term dataset to assess the sensitivity difference between various data. Did the authors compare the difference between the two datasets, and was this difference either ignored or corrected for?

Response: Thank the referee for his/her important comment. Concerning the CAMS-EGG4 product, a total of 7 satellite XCO₂ datasets are considered in the assimilation during different overlapped periods (Agusti-Panareda et al., 2022), such as CO2_IAS_NLIS (IASI), CO2_GOS_SRFP (GOSAT), and CO2_GOS_BESD (GOSAT). In our study, the XCO₂ from GOSAT and OCO-2 are adopted for the fusion from 2010 to 2020. Table r1 lists the specific information of XCO₂ from GOSAT and OCO-2. To compare their fusion performance, Figure r1 depicts the in-situ validation results of the fused results with GOSAT and OCO-2 XCO₂ during 2015-2019. As can be seen, the fusion with GOSAT XCO₂ will lead to a negative bias of -0.415 ppm and higher RMSE/σ compared to OCO-2. This suggests the usage of OCO-2 XCO₂ for the fusion after 2015 is more appropriate, which is likely attributed to its better accuracy and larger coverage. Hence, the proposed fusion method utilizes the XCO₂ from GOSAT and OCO-2 during 2010-2014 and 2015-2020, respectively. Eventually, the fused results present similar performance during two periods (see Figure r2), indicating the consistency of our long-term XCO₂ dataset.

Table r1. Specific information of XCO₂ from GOSAT and OCO-2.

Source	Scientific data record	Spatial resolution	Temporal resolution	Available period
GOSAT	"XCO2"	10.5 km (diameter)	Daily (~ 13:00 local time)	2010-2019
OCO-2	"XCO2"	1.29×2.25 km ²	Daily (~ 13:36 local time)	2015-2020

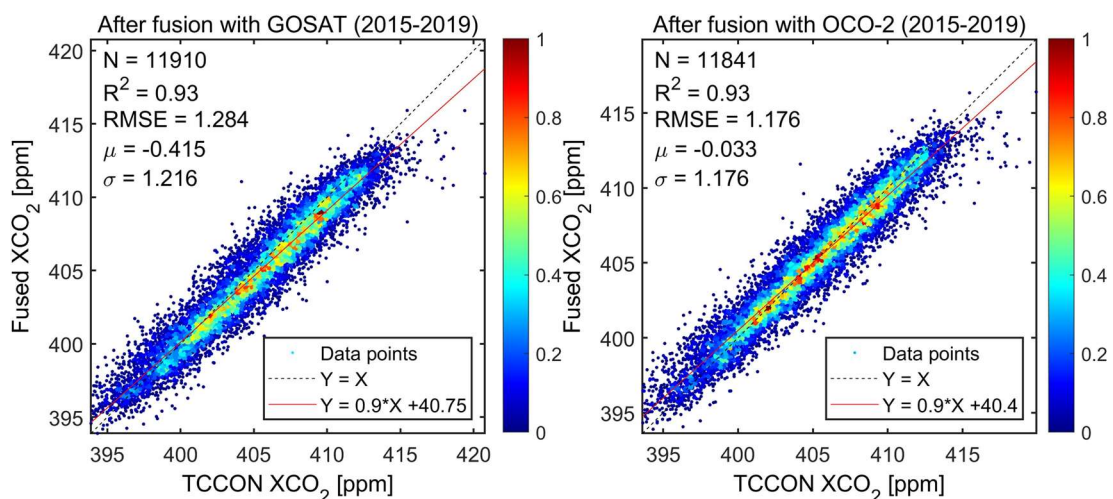


Figure r1. Density scatter-plots of the in-situ validation results for fused XCO₂ with (left) GOSAT and (right) OCO-2 from 2015 to 2019. Black dotted and red full lines stand for the 1:1 and fitted lines, respectively. Color ramps show the normalized densities of data points. X: TCCON data; Y: fused data. Unit: ppm for RMSE, μ , and σ .

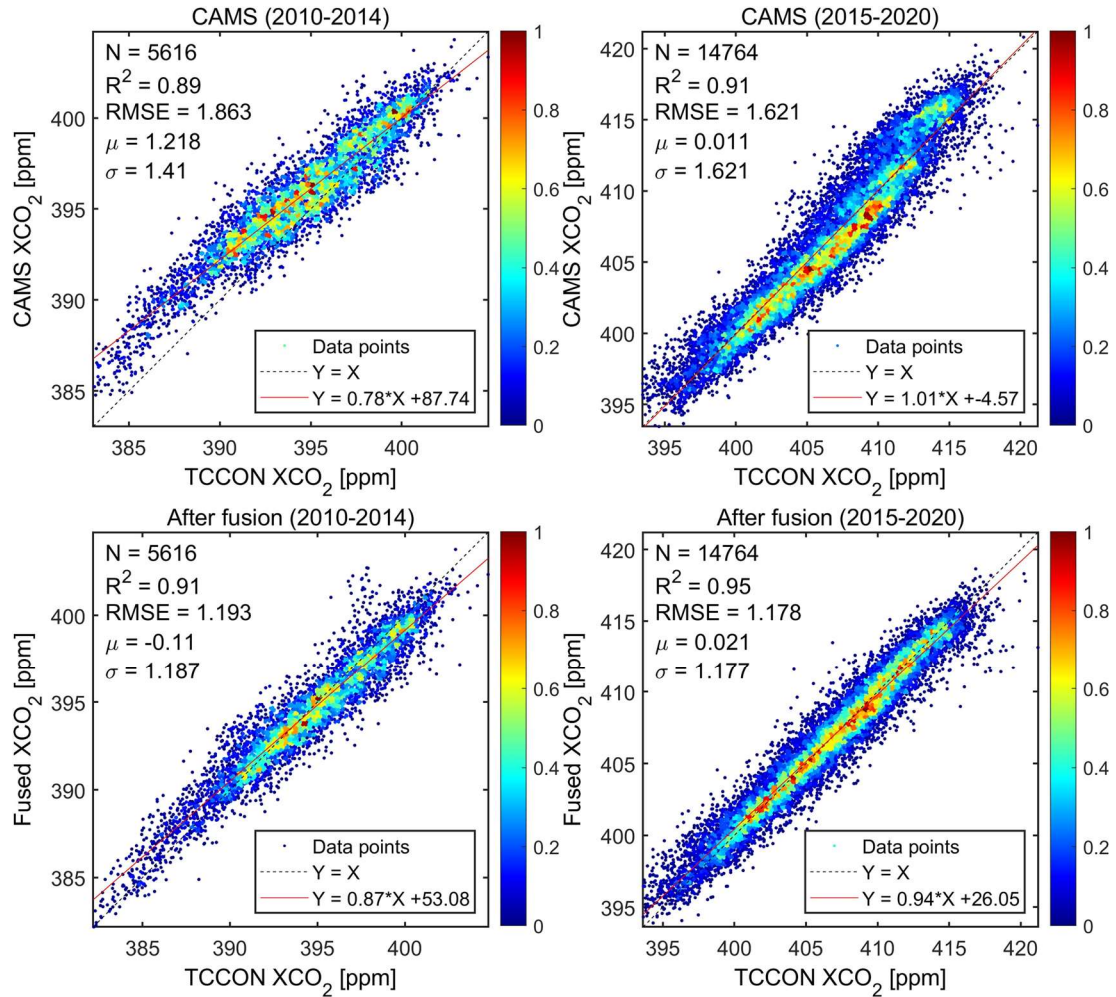


Figure r2. Density scatter-plots of the in-situ validation results for (upper) CAMS-EGG4 and (lower) fused XCO₂. Black dotted and red full lines stand for the 1:1 and fitted lines, respectively. Color ramps show the normalized densities of data points. X: TCCON data; Y: CAMS-EGG4/fused data. Unit: ppm for RMSE, μ , and σ .

Reference:

Agusti-Panareda, A., Barré, J., Massart, S., Inness, A., Aben, I., Ades, M., Baier, B. C., Balsamo, G., Borsdorff, T., Bousserez, N., Boussetta, S., Buchwitz, M., Cantarello, L., Crevoisier, C., Engelen, R., Eskes, H., Flemming, J., Garrigues, S., Hasekamp, O., Huijnen, V., Jones, L., Kipling, Z., Langerock, B., McNorton, J., Meilhac, N., Noel, S., Parrington, M., Peuch, V.-H., Ramonet, M., Ratzinger, M., Reuter, M., Ribas, R., Suttie, M., Sweeney, C., Tarniewicz, J., and Wu, L.: Technical note: The CAMS greenhouse gas reanalysis from 2003 to 2020, EGUsphere, 1–51, <https://doi.org/10.5194/egusphere-2022-283>, 2022.

Q1.3: I have some questions that are not addressed in the Methodology section. What are the range and meaning of M, N, and P in line 175? while u, v and w have the same range as i, j and

t. what's the difference and relationship between them?

Response: Thank the referee for his/her careful comment. In our study, M , N , and P represent the counts of rows (latitude), columns (longitude), and temporal sequences (days), which equal 721 (0.25° , global grids), 1441 (0.25° , global grids), and days of a year (365 or 366), respectively. Besides, i , j , and t stand for the row, column, and temporal sequence, respectively. By contrast, u , v , and w denote the transformed coordinates in frequency domain. Although u , v , and w share the same ranges with i , j , and t , their meanings are different. An example is provided in Figure r3 to show the difference and relationship between them. More related descriptions have been appended in the manuscript.

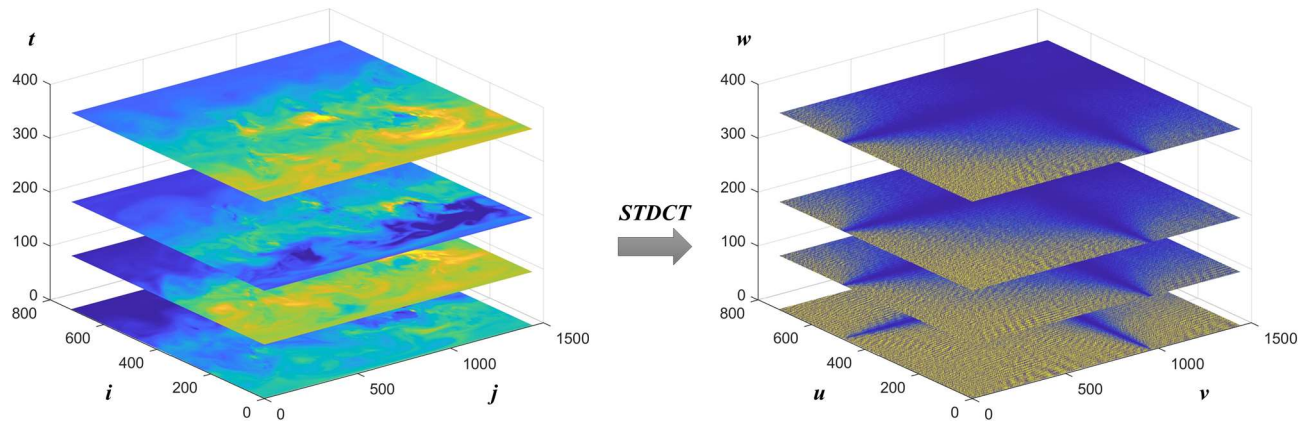


Figure r3. Comparison between CAMS-EGG4 XCO₂ and its transformed three-dimensional tensor after STDCT in 2015.

The main revision is as follows:

M , N , and P stand for the counts of rows (latitude), columns (longitude), and temporal sequences (days), which equal 721 (0.25° , global grids), 1441 (0.25° , global grids), and days of a year (365 or 366), respectively.

Q1.4: In the Equation 4, δ represents a series of values or a three-dimensional tensor. Based on Equations 5 and 6, it appears that δ is a tensor. How are positions without values in δ handled and does it affect the final iteration process?

Response: Thank the referee for his/her comment. δ is defined as a three-dimensional tensor, of which the values are only available when satellite XCO₂/XCH₄ products are valid. In our study, the proposed fusion method can reconstruct the missing information in δ using its available values. Specific procedures are as follows:

- (1) Initialize missing values in δ through the spatiotemporal nearest neighbor interpolation.

- (2) Update δ by iterations with Eq. (6) based on the spatiotemporal knowledge of self-correlation. Retain the original available values of δ after each iteration.
- (3) Repeat procedure (2) until the number of total iterations or error reaches a predetermined threshold. A schematic diagram to demonstrate the iteration process of δ (fusion with OCO-2 XCO₂) in 2017-04-10 is depicted in Figure r4.

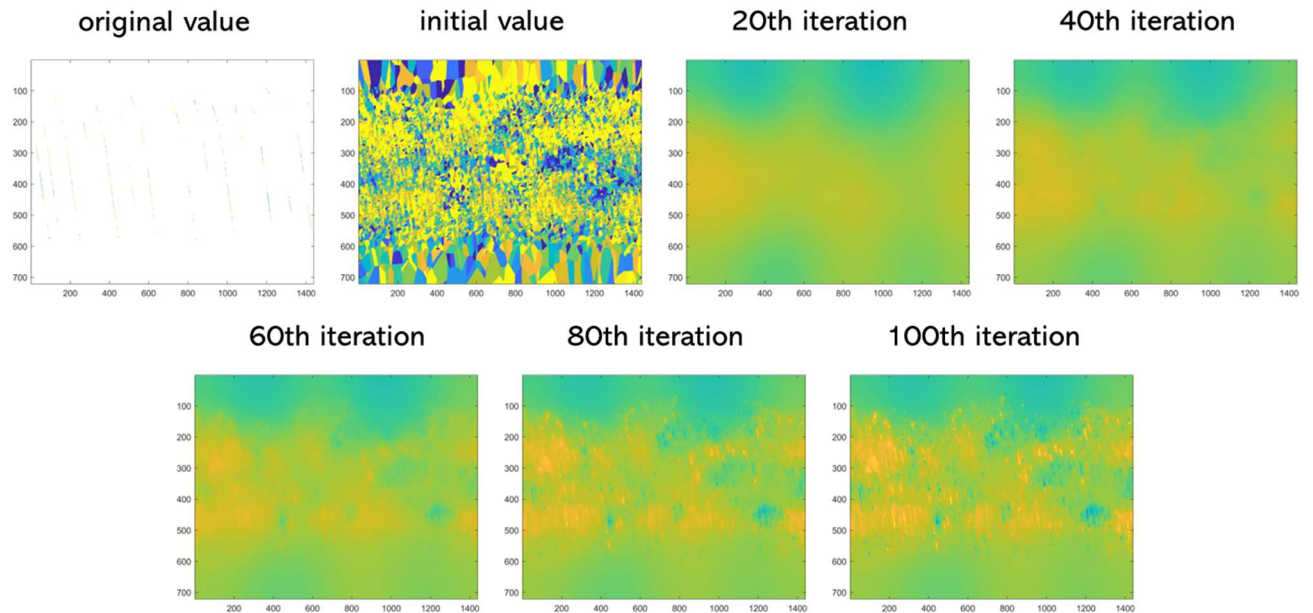


Figure r4. Schematic diagram to show the iteration process of δ (fusion with OCO-2 XCO₂) in 2017-04-10.

Q1.5: I am curious that the configuration of the parameters in line 208. How do these parameters affect the results, especially for ε ?

Response: Thank the referee for his/her comment. The number of total iterations affects the performance of fused results. The fusion performance firstly increases as the number of total iterations rises and then tends to be relatively stable. γ is a relaxation factor to accelerate convergence. The convergence will be faster as γ grows up. However, a large γ may magnify the error of convergence. ε represents a smoothing factor. A large γ value could result in the loss of high-frequency components (Garcia, 2010). This parameter generally needs to be smaller and smaller to reduce the influence of smoothing during the iterations.

Reference:

Garcia, D.: Robust smoothing of gridded data in one and higher dimensions with missing values, Computational Statistics & Data Analysis, 54, 1167–1178, <https://doi.org/10.1016/j.csda.2009.09.020>, 2010.

Technical corrections:

Q1.6: L21: The full name of σ and R^2 .

Response: Thank the referee for his/her comment. The full name of σ and R^2 have been appended in Line 21.

The main revision is as follows:

Validation results show that the proposed method achieves a satisfactory accuracy, with the Standard-Deviation of Bias (σ) of ~ 1.18 ppm for XCO₂ and 11.3 ppb for XCH₄ against TCCON measurements from 2010 to 2020. Meanwhile, the Determination-Coefficient (R^2) of XCO₂ and XCH₄ reach 0.91/0.95 (2010-2014/2015-2020) and 0.9 (2010-2020) after fusion, respectively.

Q1.7: L21-22: Why the R^2 of XCO₂ against TCCON measurements is given as a range, while the R^2 of XCH₄ is a single number? They should be consistent.

Response: Thank the referee for his/her comment. The R^2 of XCO₂ against TCCON measurements has been revised in the manuscript.

The main revision is as follows:

Validation results show that the proposed method achieves a satisfactory accuracy, with the Standard-Deviation of Bias (σ) of ~ 1.18 ppm for XCO₂ and 11.3 ppb for XCH₄ against TCCON measurements from 2010 to 2020. Meanwhile, the Determination-Coefficient (R^2) of XCO₂ and XCH₄ reach 0.91/0.95 (2010-2014/2015-2020) and 0.9 (2010-2020) after fusion, respectively.

Q1.8: L117: The full name of QA. It is the first mention in this text.

Response: Thank the referee for his/her comment. The full name of QA was given in Line 127 by mistake and has been moved to Line 117.

The main revision is as follows:

Furthermore, the quality assurance (QA) records of “XCO₂ Quality Flag” and “XCH₄ Quality Flag” are exploited to filter

bad data.

Q1.9: L349: R^2 : 0.91 or 0.95 means the results of GOSAT and OCO-2? This sentence can be expressed more clearly.

Response: Thank the referee for his/her comment. This sentence has been reworded to be more clearly.

The main revision is as follows:

Validation results show that the S-STDCT fusion method performs well over the globe, with the σ of ~ 1.18 ppm for XCO₂ and 11.3 ppb for XCH₄ against TCCON measurements during 2010-2020. Meanwhile, the R^2 of fused XCO₂ and XCH₄ reach 0.91/0.95 (2010-2014/2015-2020) and 0.9 (2010-2020), respectively.

Q1.10: Figures: Modify the superscript of R^2 and subscript of XCO₂ and XCH₄ in all Figures.

Response: Thank the referee for his/her careful comment. The superscript of R^2 and subscript of XCO₂ and XCH₄ have been modified in all figures.

The main revision is as follows:

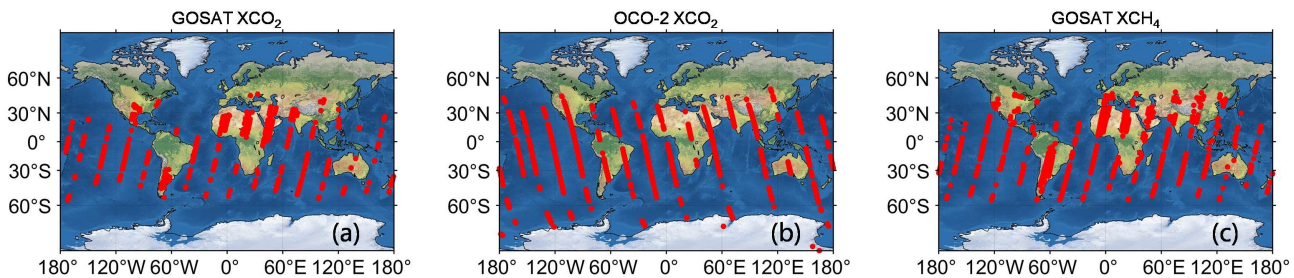


Figure 1. An example of daily spatial footprints for (a) GOSAT XCO₂, (b) OCO-2 XCO₂, and (c) GOSAT XCH₄. Red points signify the available data. Background maps are naturally shaded reliefs over the globe.

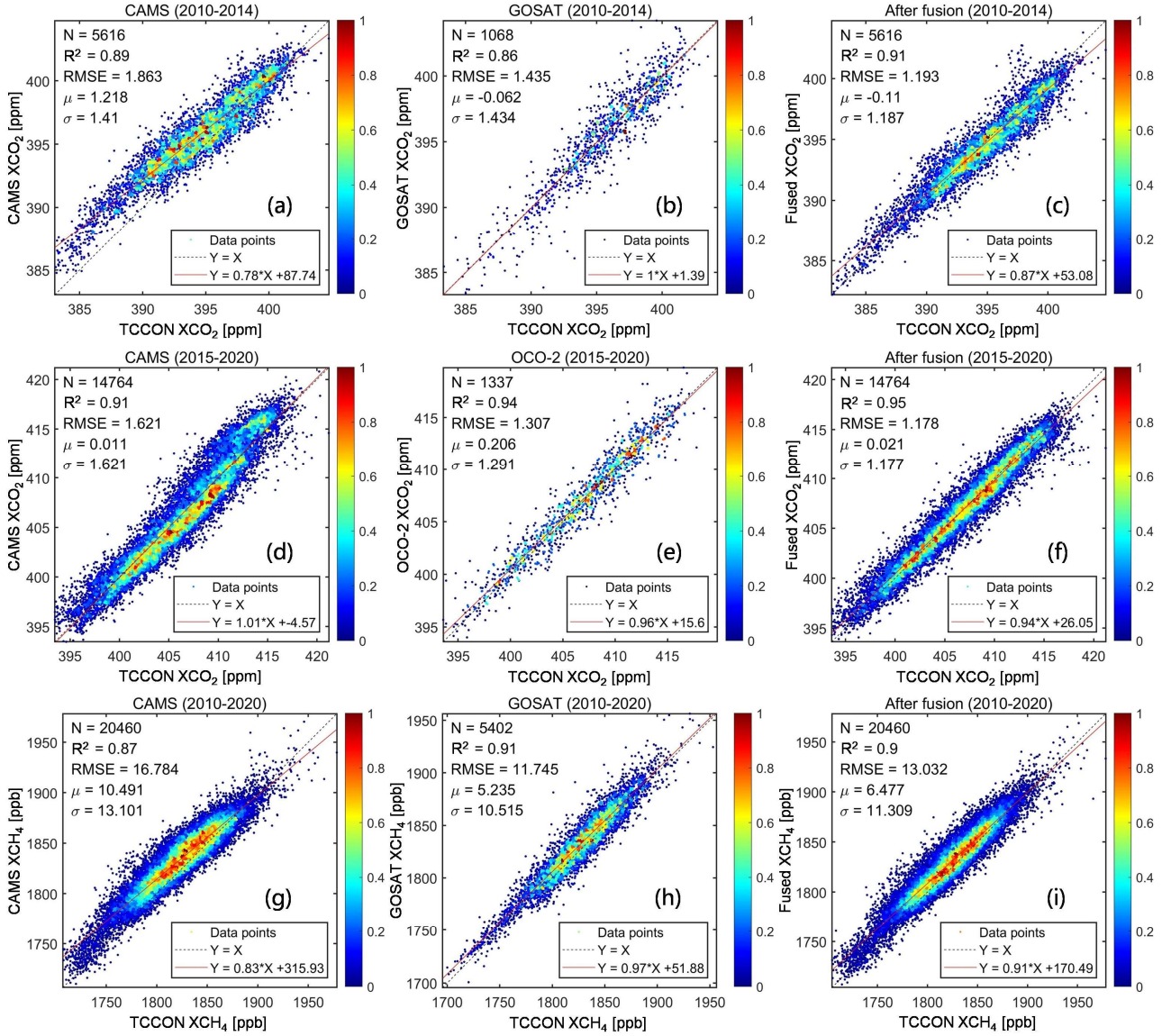


Figure 3. Density scatter-plots of the in-situ validation results for (a, d, and g) CAMS-EGG4, (b and h) GOSAT, (e) OCO-2, and (c, f, and i) fused results. Black dotted and red full lines stand for the 1:1 and fitted lines, respectively. Color ramps show the normalized densities of data points. X: TCCON data; Y: CAMS-EGG4/GOSAT/OCO-2/fused data. Unit: ppm/ppb to XCO₂/XCH₄ for RMSE, μ , and σ .

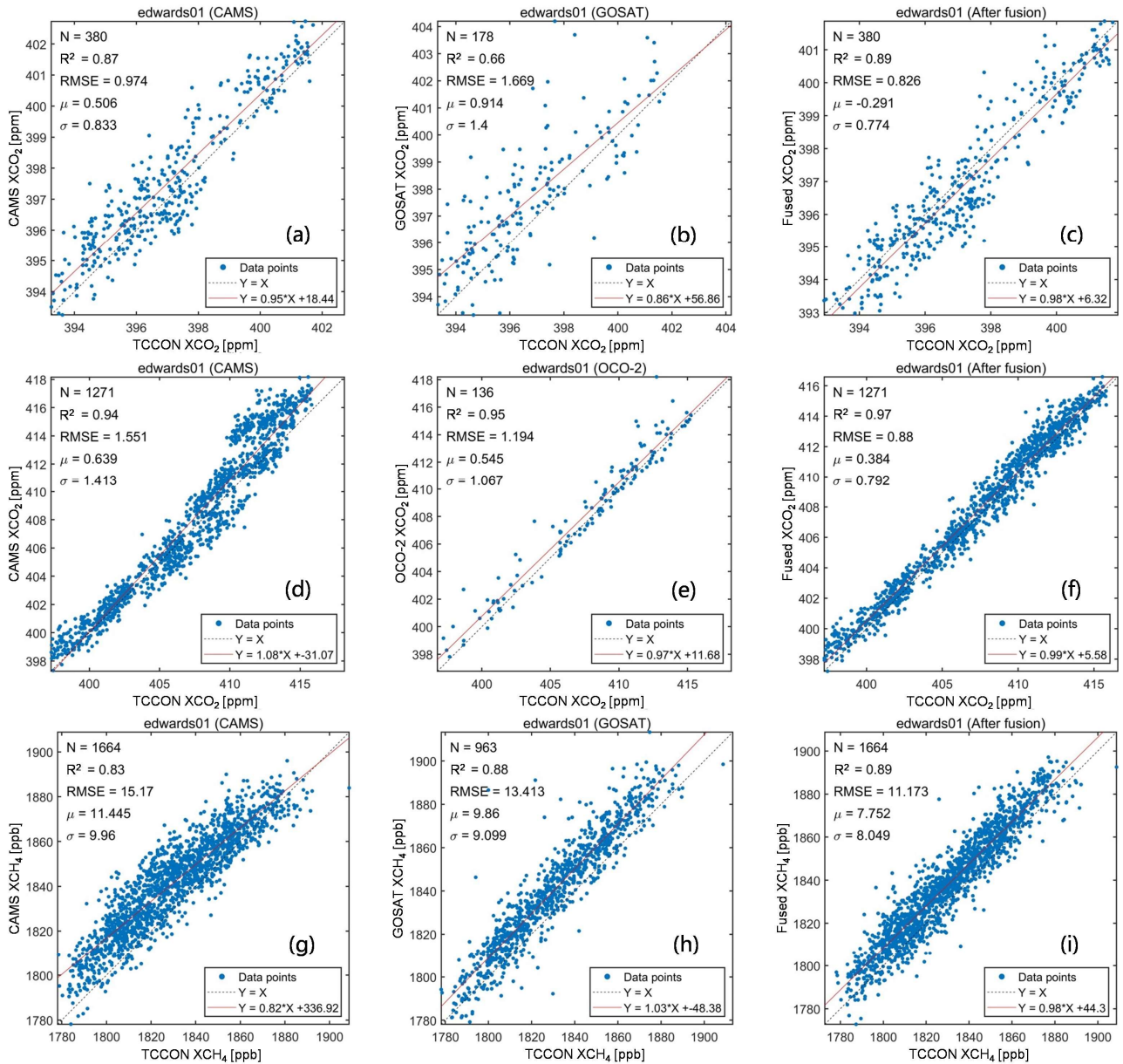


Figure 4. Scatter-plots of the in-situ validation results for (a, d, and g) CAMS-EGG4, (b and h) GOSAT, (e) OCO-2, and (c, f, and i) fused results on edwards01. Black dotted and red full lines stand for the 1:1 and fitted lines, respectively. X: TCCON data; Y: CAMS-EGG4/GOSAT/OCO-2/fused data. Unit: ppm/ppb to XCO₂/XCH₄ for RMSE, μ , and σ .

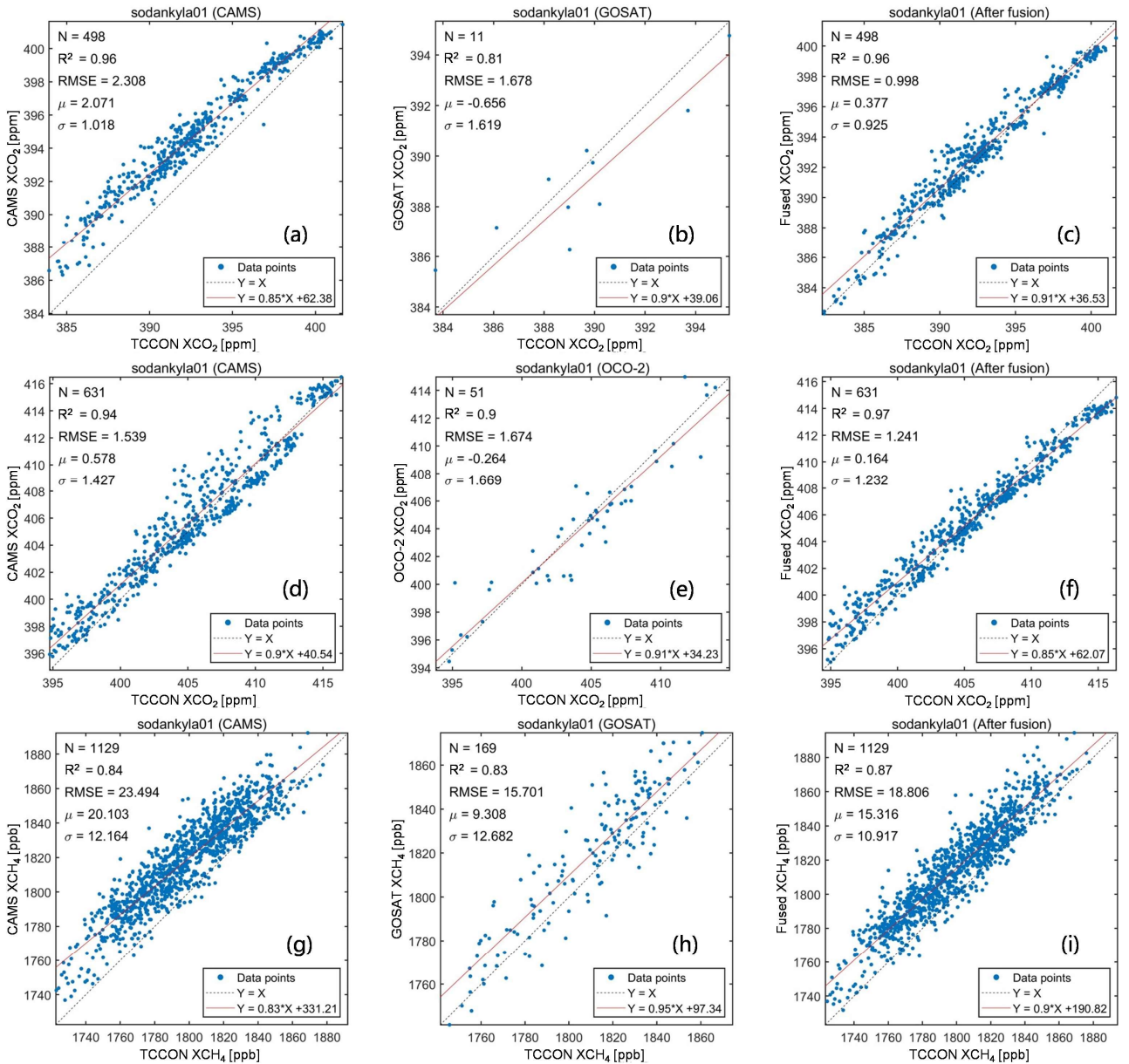


Figure 5. Scatter-plots of the in-situ validation results for (a, d, and g) CAMS-EGG4, (b and h) GOSAT, (e) OCO-2, and (c, f, and i) fused results on sodankyla01. Black dotted and red full lines stand for the 1:1 and fitted lines, respectively. X: TCCON data; Y: CAMS-EGG4/GOSAT/OCO-2/fused data. Unit: ppm/ppb to XCO₂/XCH₄ for RMSE, μ , and σ .

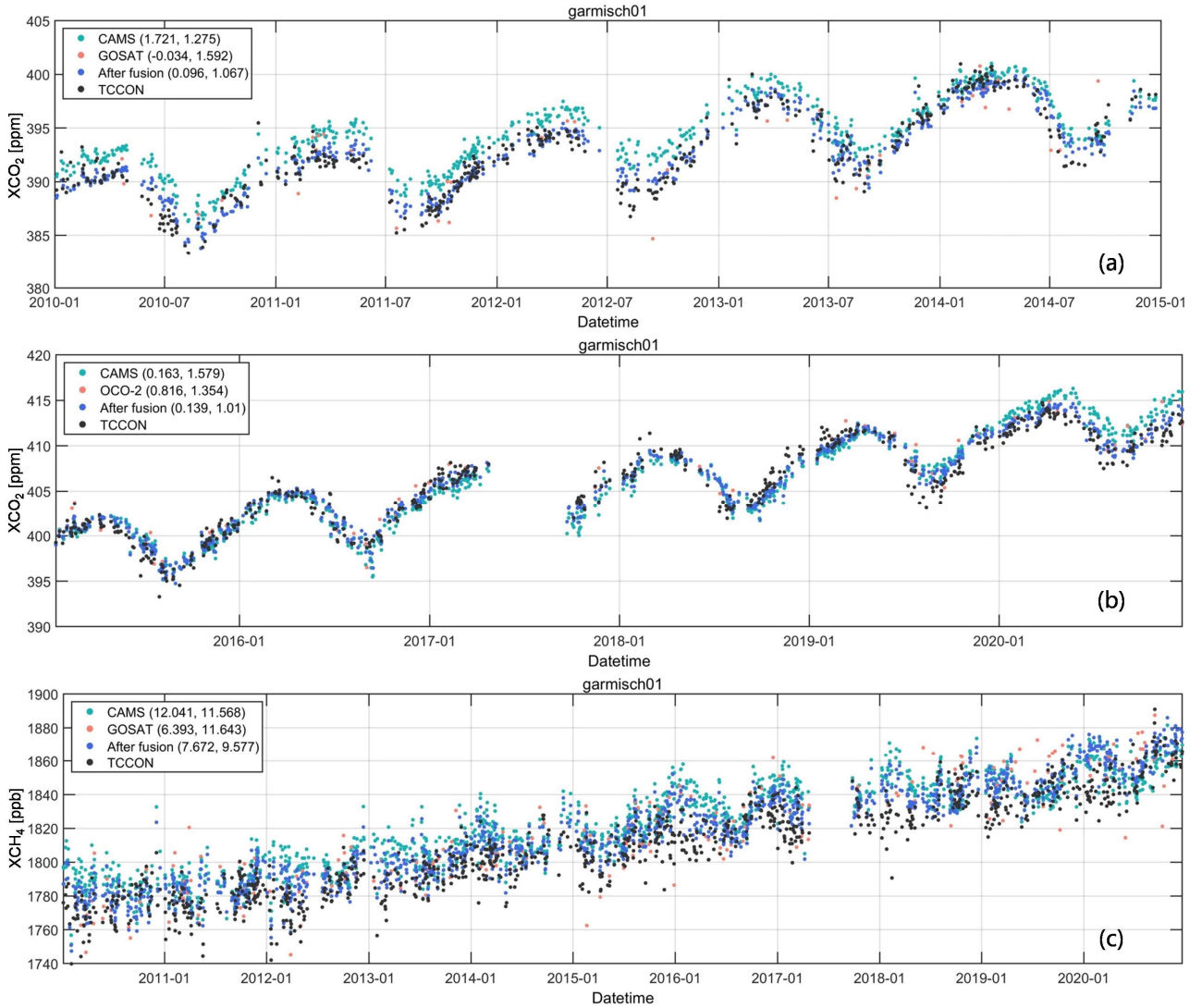


Figure 6. Scatter-plots of the time series for daily CAMS-EGG4, GOSAT, OCO-2, fused, and TCCON data on garmisch01. The first and second numbers in the bracket represent μ and σ , respectively. Unit: ppm/ppb to XCO₂/XCH₄ for μ and σ .

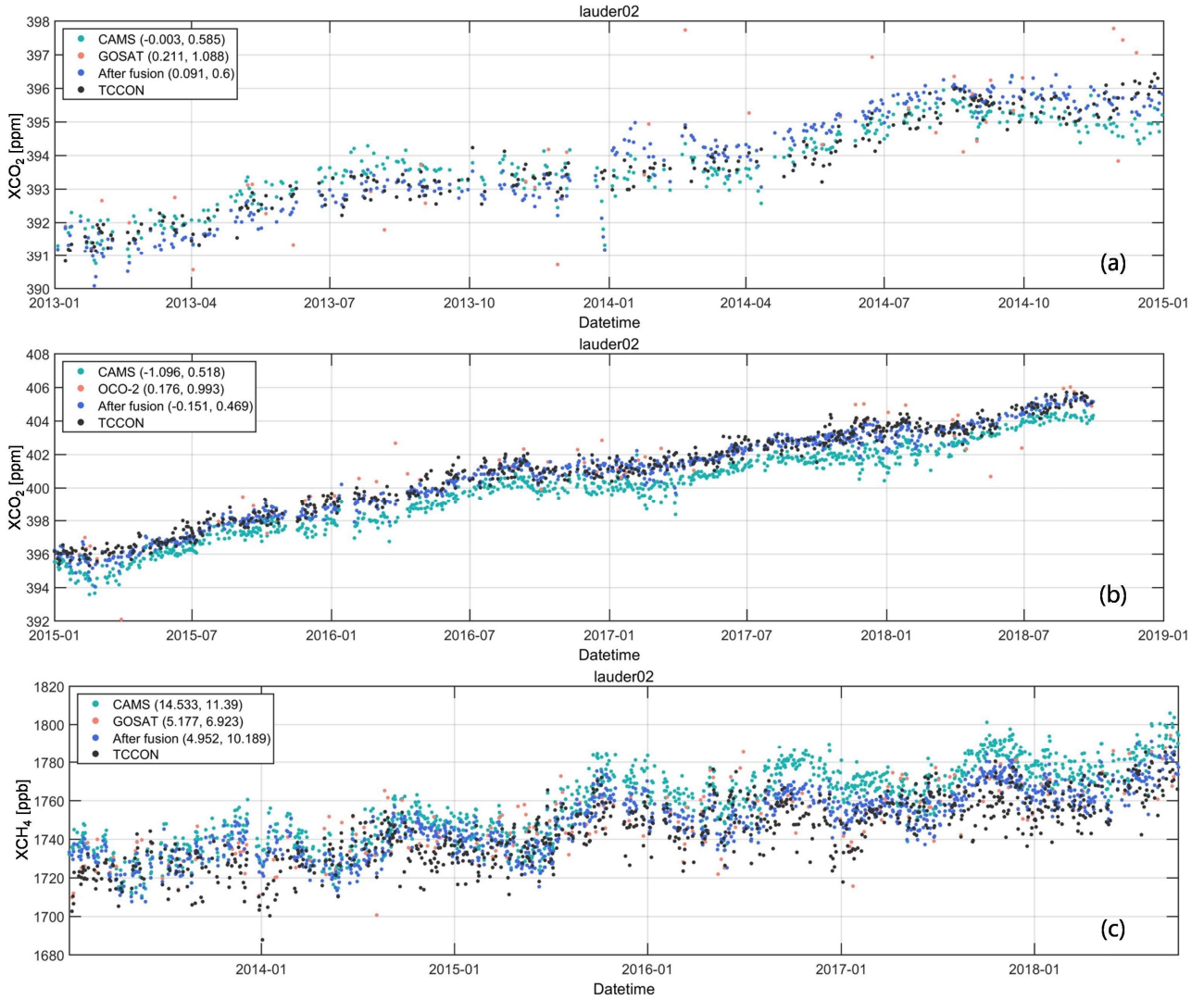


Figure 7. Scatter-plots of the time series for daily CAMS-EGG4, GOSAT, OCO-2, fused, and TCCON data on lauder02. The first and second numbers in the bracket represent μ and σ , respectively. Unit: ppm/ppb to $\text{XCO}_2/\text{XCH}_4$ for μ and σ .

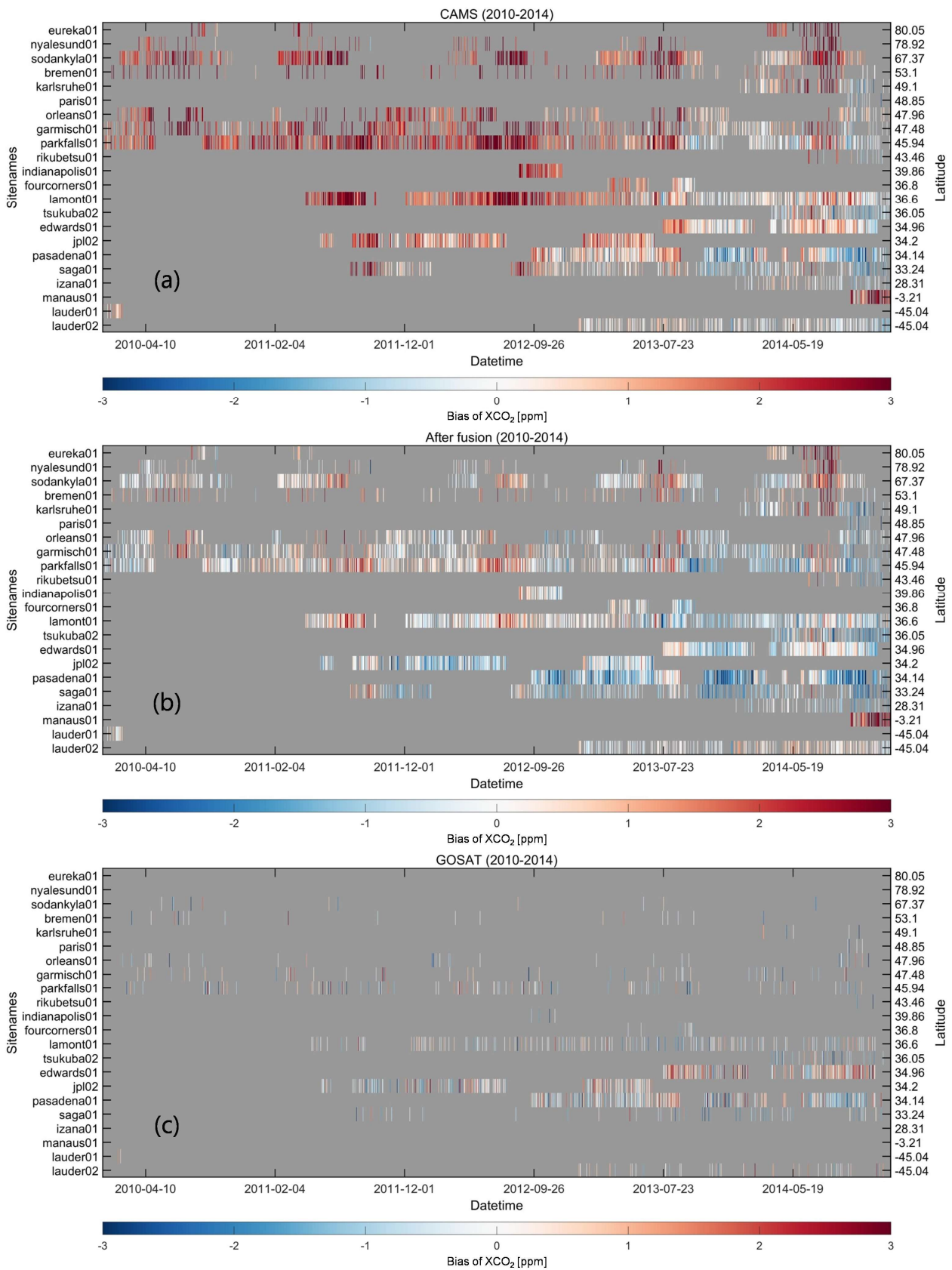


Figure 8. Heat maps of the biases between daily (a) CAMS-EGG4/(b) fused/(c) GOSAT and TCCON XCO₂ over time and latitude. Color ramps stand for the biases of XCO₂. Background colors (grey) indicate the missing data.

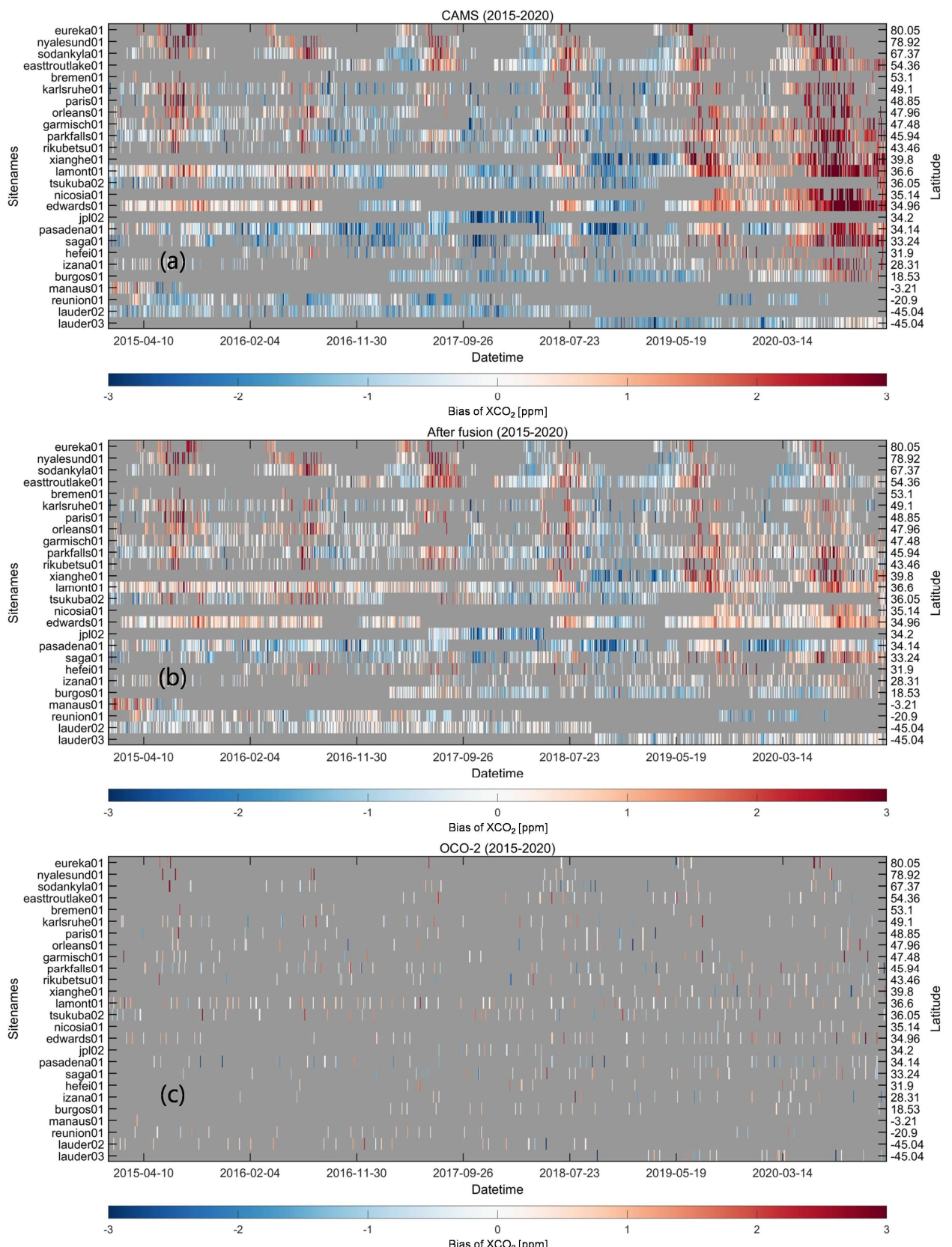


Figure 9. Heat maps of the biases between daily (a) CAMS-EGG4/(b) fused/(c) OCO-2 and TCCON XCO_2 over time and latitude. Color ramps stand for the biases of XCO_2 . Background colors (grey) indicate the missing data.

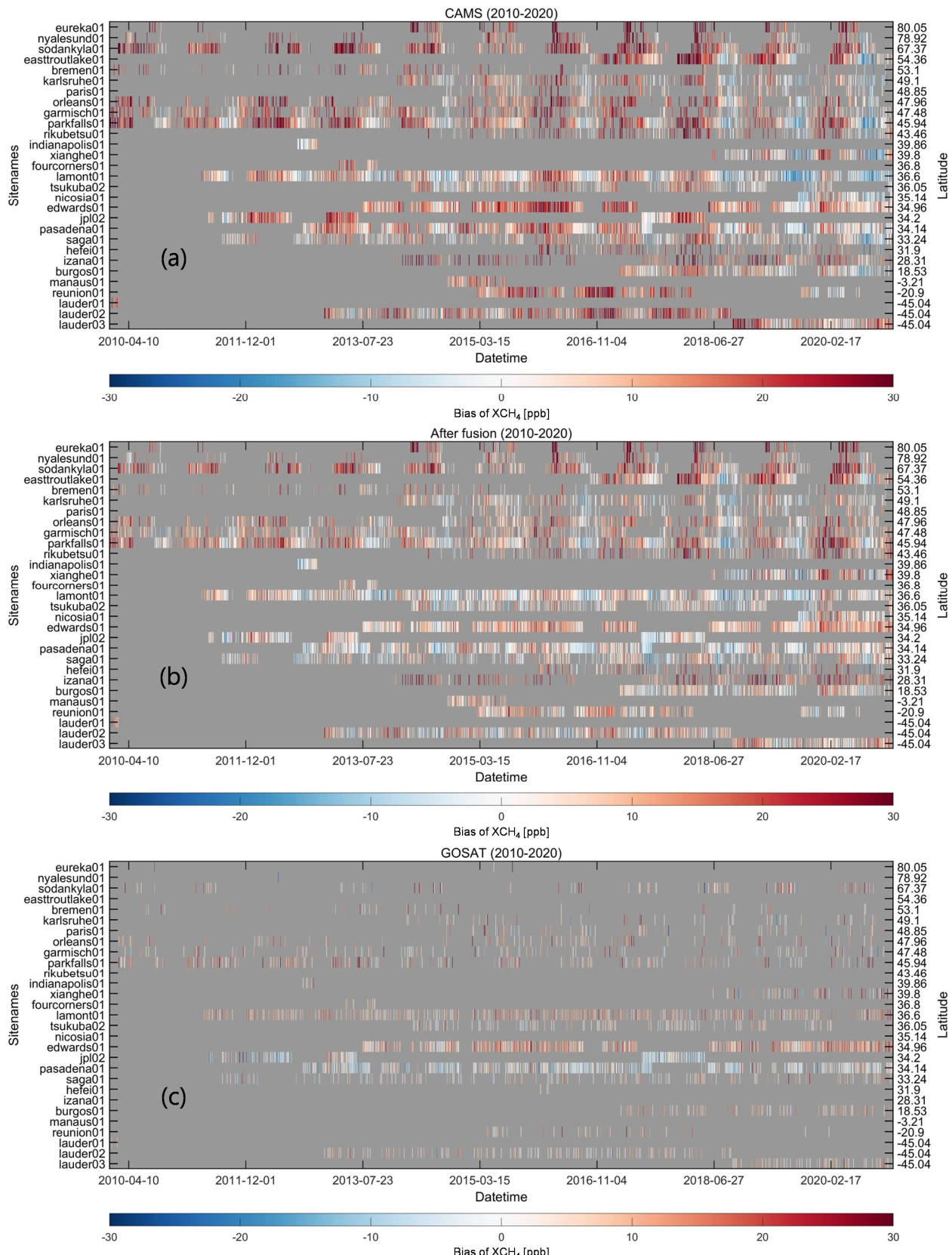


Figure 10. Heat maps of the biases between daily (a) CAMS-EGG4/(b) fused/(c) GOSAT and TCCON XCH_4 over time and latitude. Color ramps stand for the biases of XCO_2 . Background colors (grey) indicate the missing data.

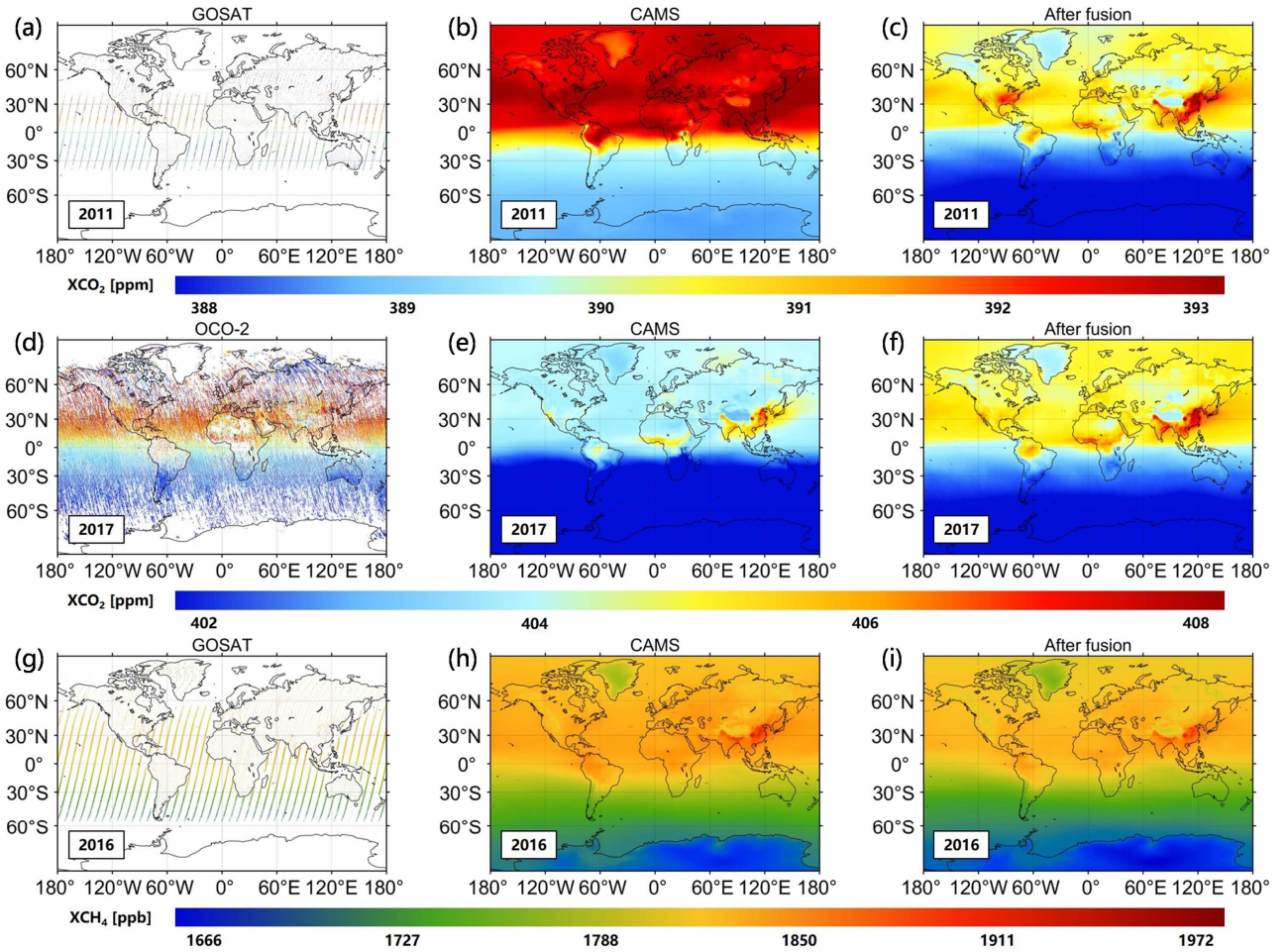


Figure 11. Annual (a and g) GOSAT, (d) OCO-2, (b, e, and h) CAMS-EGG4, and (c, f, and i) fused XCO₂/XCH₄ over the globe. Color ramps stand for the values of XCO₂ and XCH₄.

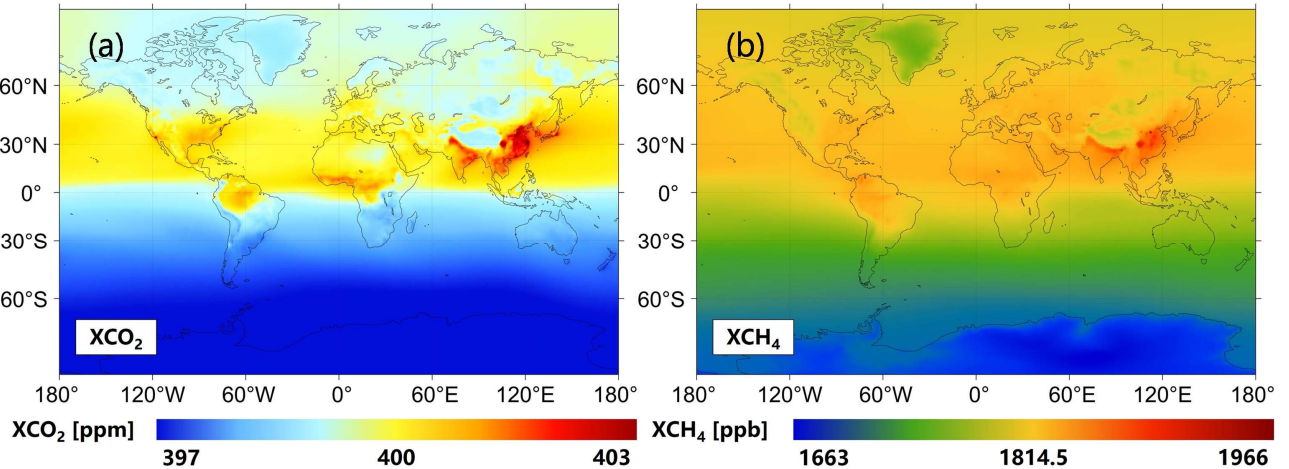


Figure 14. Multi-year mean fused (a) XCO₂ and (b) XCH₄ from 2010 to 2020 over the globe. Color ramps stand for the values of XCO₂ and XCH₄.

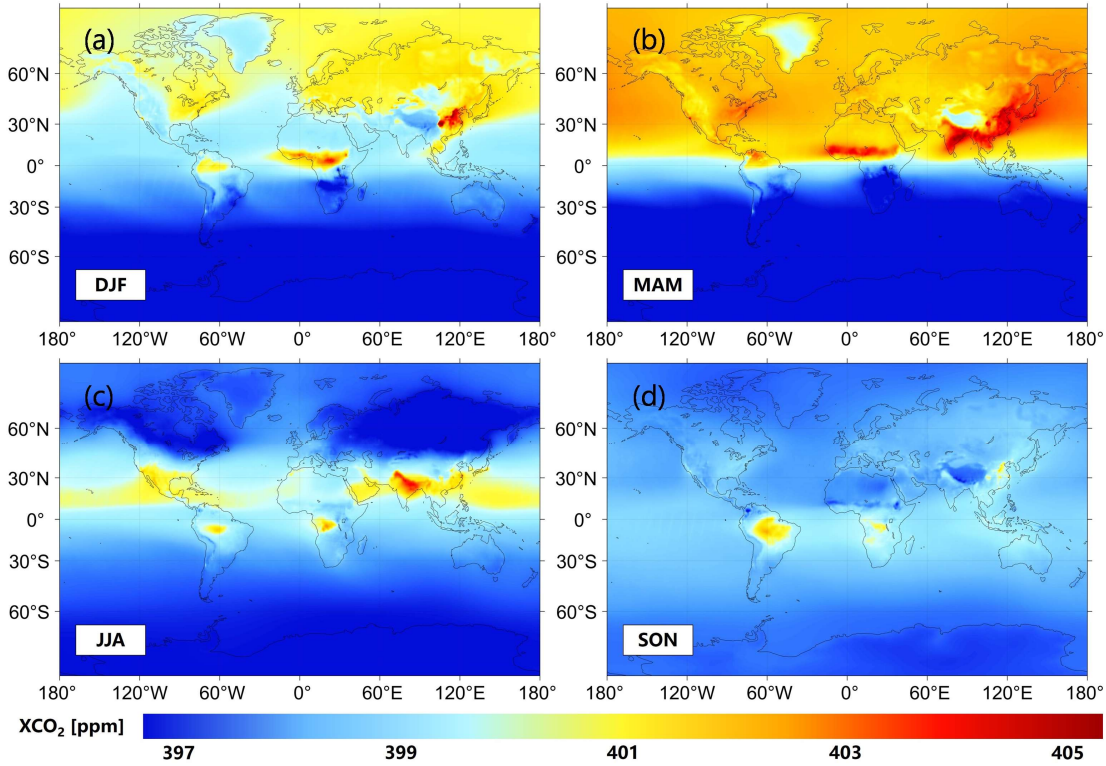


Figure 15. Seasonal fused XCO₂ from 2010 to 2020 over the globe. The color ramp stands for the value of XCO₂. (a) DJF, (b) MAM, (c) JJA, and (d) SON denote Dec. to Feb., Mar. to May., Jun. to Aug., and Sep. to Nov., respectively.

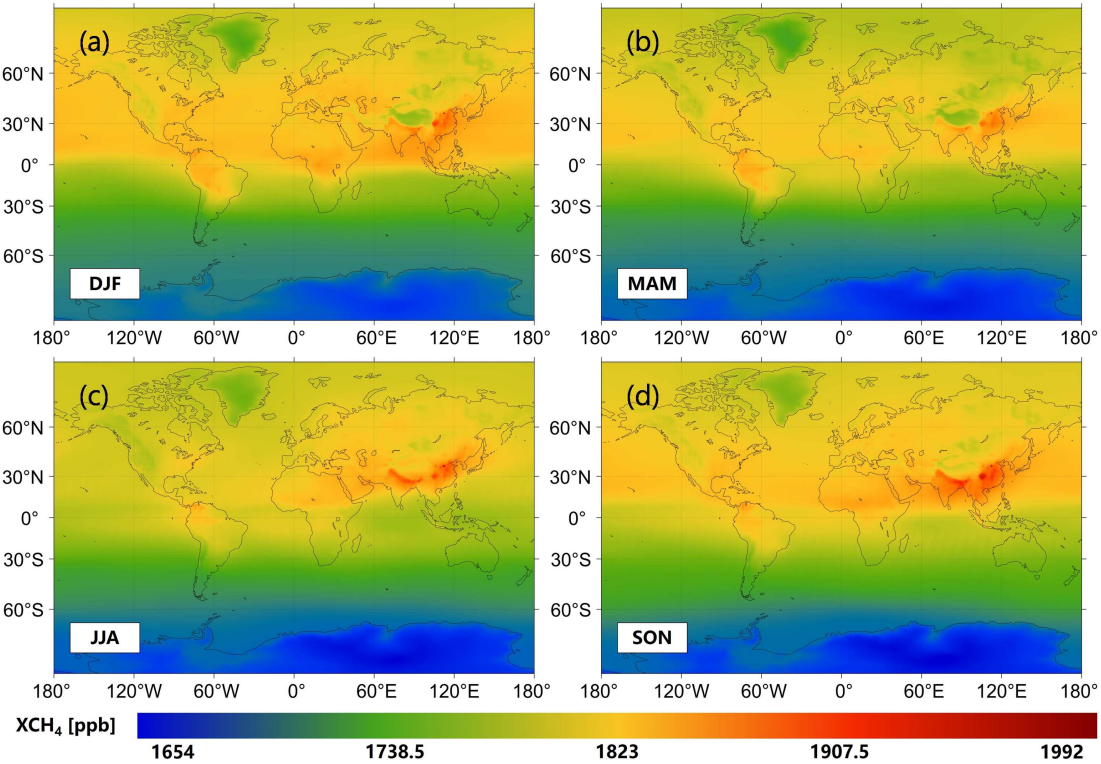


Figure 16. Seasonal fused XCH₄ from 2010 to 2020 over the globe. The color ramp stands for the value of XCH₄. (a) DJF, (b) MAM, (c) JJA, and (d) SON denote Dec. to Feb., Mar. to May., Jun. to Aug., and Sep. to Nov., respectively.

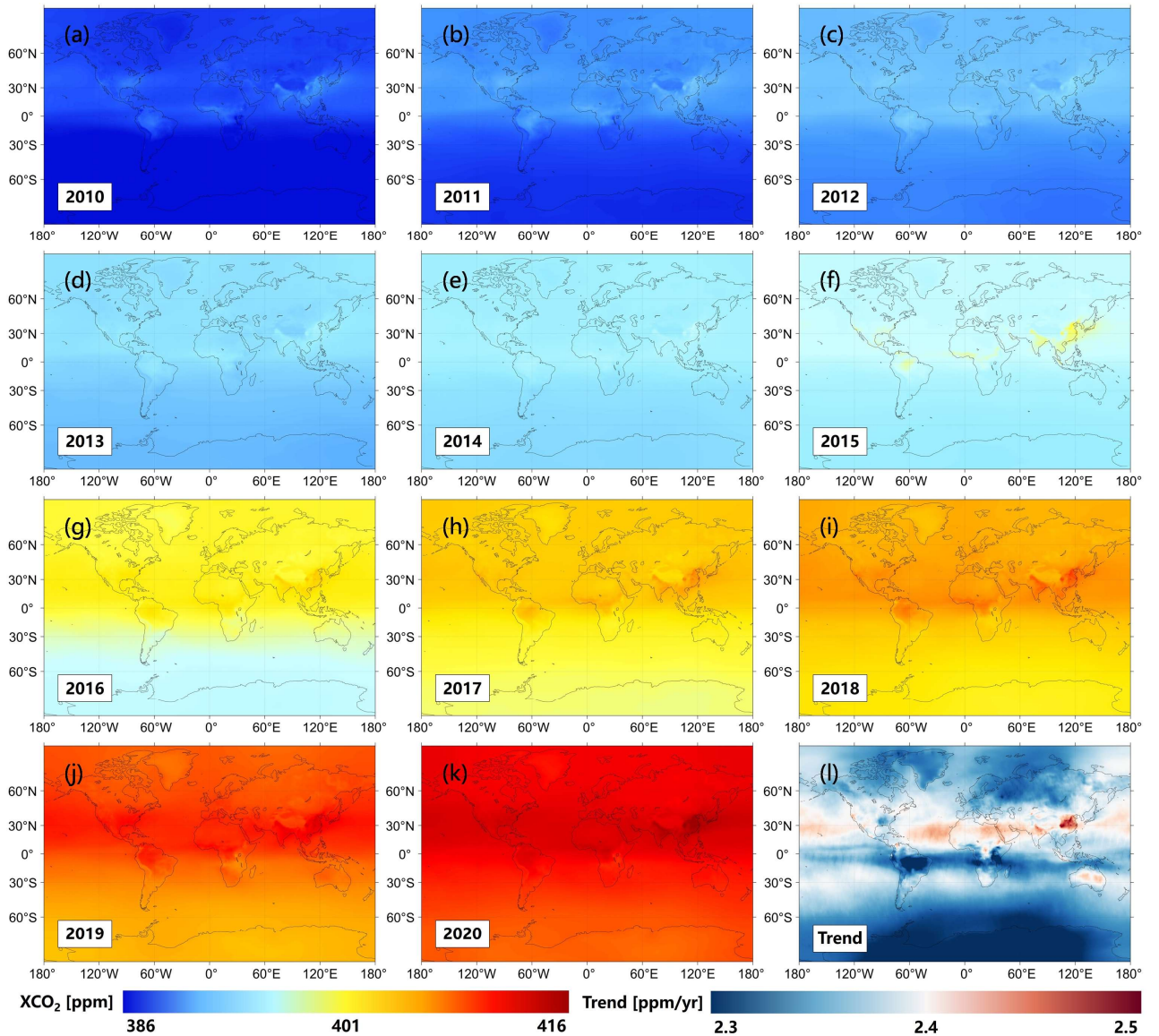


Figure 17. Annual fused (a-k) XCO₂ and (l) its trend from 2010 to 2020 over the globe. Color ramps stand for the values of XCO₂ and its trend. ppm/yr: ppm per year.

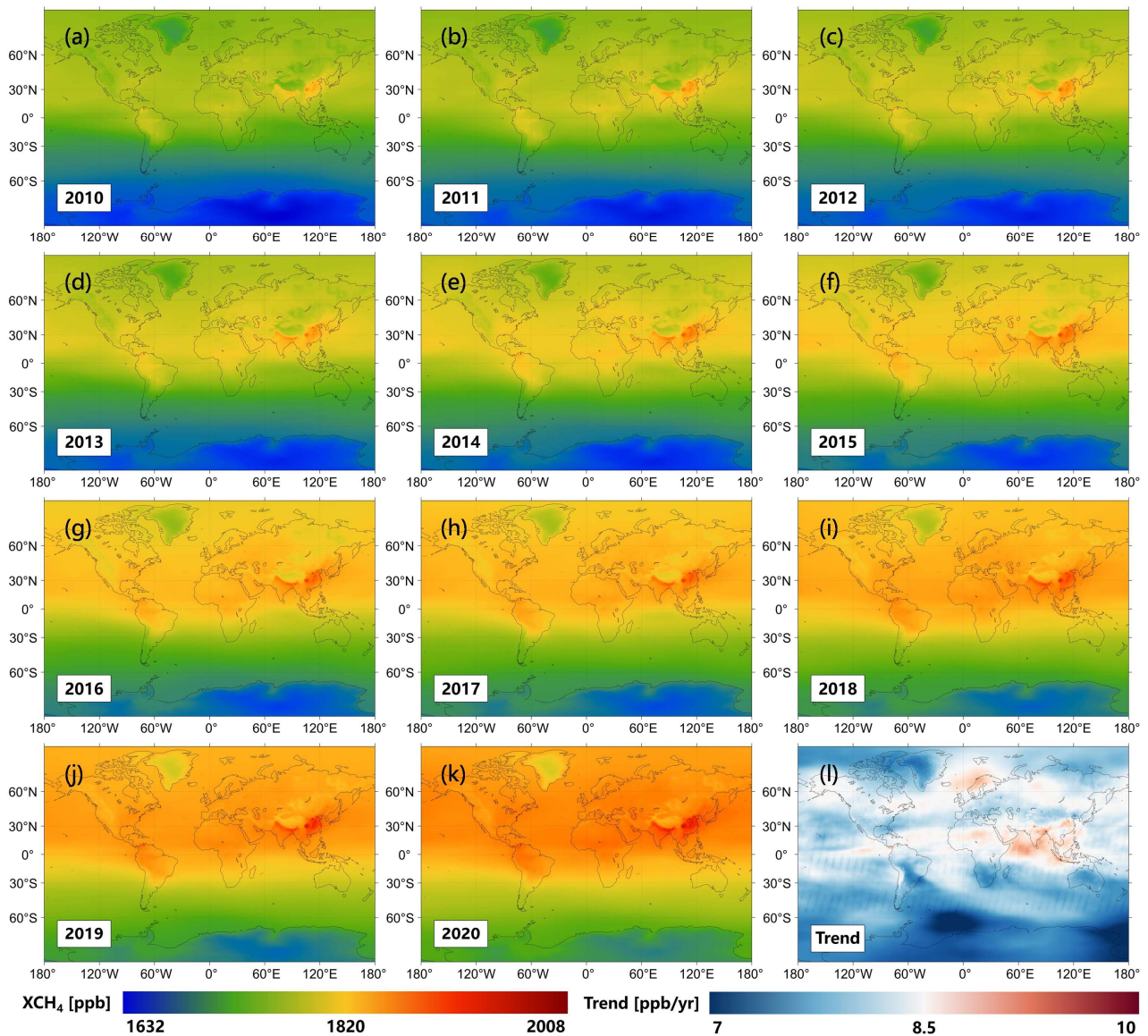


Figure 18. Annual fused (a-k) XCH₄ and (l) its trend from 2010 to 2020 over the globe. Color ramps stand for the values of XCH₄ and its trend. ppb/yr: ppb per year.

Q1.11: Text: Figure and Fig. need to be unified.

Response: Thank the referee for his/her comment. In our study, the text formats of figures (i.e., “Figure” and “Fig.”) followed the submission instructions of ESSD (<https://www.earth-system-science-data.net/submission.html#figurestables>):

- The abbreviation "Fig." should be used when it appears in running text and should be followed by a number unless it comes at the beginning of a sentence, e.g.: "The results are depicted in Fig. 5. Figure 9 reveals that...".

Q1.12: References: Modify the subscript of all references.

Response: Thank the referee for his/her comment. The subscript of all references has been modified.

The main revision is as follows:

Bergamaschi, P., Houweling, S., Segers, A., Krol, M., Frankenberg, C., Scheepmaker, R. A., Dlugokencky, E., Wofsy, S. C., Kort, E. A., Sweeney, C., Schuck, T., Brenninkmeijer, C., Chen, H., Beck, V., and Gerbig, C.: Atmospheric CH₄ in the first decade of the 21st century: Inverse modeling analysis using SCIAMACHY satellite retrievals and NOAA surface measurements, *Journal of Geophysical Research: Atmospheres*, 118, 7350–7369, <https://doi.org/10.1002/jgrd.50480>, 2013.

Buchwitz, M., Reuter, M., Schneising, O., Boesch, H., Guerlet, S., Dils, B., Aben, I., Armante, R., Bergamaschi, P., Blumenstock, T., Bovensmann, H., Brunner, D., Buchmann, B., Burrows, J. P., Butz, A., Chédin, A., Chevallier, F., Crevoisier, C. D., Deutscher, N. M., Frankenberg, C., Hase, F., Hasekamp, O. P., Heymann, J., Kaminski, T., Laeng, A., Lichtenberg, G., De Mazière, M., Noël, S., Notholt, J., Orphal, J., Popp, C., Parker, R., Scholze, M., Sussmann, R., Stiller, G. P., Warneke, T., Zehner, C., Bril, A., Crisp, D., Griffith, D. W. T., Kuze, A., O'Dell, C., Oshchepkov, S., Sherlock, V., Suto, H., Wennberg, P., Wunch, D., Yokota, T., and Yoshida, Y.: The Greenhouse Gas Climate Change Initiative (GHG-CCI): Comparison and quality assessment of near-surface-sensitive satellite-derived CO₂ and CH₄ global data sets, *Remote Sensing of Environment*, 162, 344–362, <https://doi.org/10.1016/j.rse.2013.04.024>, 2015.

Chen, H., Xu, X., Fang, C., Li, B., and Nie, M.: Differences in the temperature dependence of wetland CO₂ and CH₄ emissions vary with water table depth, *Nat. Clim. Chang.*, 11, 766–771, <https://doi.org/10.1038/s41558-021-01108-4>, 2021.

Hakkainen, J., Ialongo, I., and Tamminen, J.: Direct space-based observations of anthropogenic CO₂ emission areas from OCO-2, *Geophysical Research Letters*, 43, 11,400–11,406, <https://doi.org/10.1002/2016GL070885>, 2016.

He, C., Ji, M., Grieneisen, M. L., and Zhan, Y.: A review of datasets and methods for deriving spatiotemporal distributions of atmospheric CO₂, *Journal of Environmental Management*, 322, 116101, <https://doi.org/10.1016/j.jenvman.2022.116101>, 2022a.

He, C., Ji, M., Li, T., Liu, X., Tang, D., Zhang, S., Luo, Y., Grieneisen, M. L., Zhou, Z., and Zhan, Y.: Deriving Full-Coverage and Fine-Scale XCO₂ Across China Based on OCO-2 Satellite Retrievals and CarbonTracker Output, *Geophysical Research Letters*, 49, e2022GL098435, <https://doi.org/10.1029/2022GL098435>, 2022b.

He, Z., Lei, L., Zhang, Y., Sheng, M., Wu, C., Li, L., Zeng, Z.-C., and Welp, L. R.: Spatio-Temporal Mapping of Multi-Satellite Observed Column Atmospheric CO₂ Using Precision-Weighted Kriging Method, *Remote Sensing*, 12, 576, <https://doi.org/10.3390/rs12030576>, 2020.

Hotchkiss, E. R., Hall Jr, R. O., Sponseller, R. A., Butman, D., Klaminder, J., Laudon, H., Rosvall, M., and Karlsson, J.: Sources of and processes controlling CO₂ emissions change with the size of streams and rivers, *Nature Geosci*, 8, 696–699, <https://doi.org/10.1038/ngeo2507>, 2015.

Houweling, S., Baker, D., Basu, S., Boesch, H., Butz, A., Chevallier, F., Deng, F., Dlugokencky, E. J., Feng, L.,

Ganshin, A., Hasekamp, O., Jones, D., Maksyutov, S., Marshall, J., Oda, T., O'Dell, C. W., Oshchepkov, S., Palmer, P. I., Peylin, P., Poussi, Z., Reum, F., Takagi, H., Yoshida, Y., and Zhuravlev, R.: An intercomparison of inverse models for estimating sources and sinks of CO₂ using GOSAT measurements, *Journal of Geophysical Research: Atmospheres*, 120, 5253–5266, <https://doi.org/10.1002/2014JD022962>, 2015.

Katzfuss, M. and Cressie, N.: Tutorial on fixed rank kriging (FRK) of CO₂ data, Department of Statistics, The Ohio State University, Columbus, 2011.

Kenea, S. T., Lee, H., Patra, P. K., Li, S., Labzovskii, L. D., and Joo, S.: Long-term changes in CH₄ emissions: Comparing ΔCH₄/ΔCO₂ ratios between observation and proved model in East Asia (2010–2020), *Atmospheric Environment*, 293, 119437, <https://doi.org/10.1016/j.atmosenv.2022.119437>, 2023.

Le Quéré, C., Korsbakken, J. I., Wilson, C., Tosun, J., Andrew, R., Andres, R. J., Canadell, J. G., Jordan, A., Peters, G. P., and van Vuuren, D. P.: Drivers of declining CO₂ emissions in 18 developed economies, *Nat. Clim. Chang.*, 9, 213–217, <https://doi.org/10.1038/s41558-019-0419-7>, 2019.

Li, L., Lei, L., Song, H., Zeng, Z., and He, Z.: Spatiotemporal Geostatistical Analysis and Global Mapping of CH₄ Columns from GOSAT Observations, *Remote Sensing*, 14, 654, <https://doi.org/10.3390/rs14030654>, 2022.

Liu, J., Fung, I., Kalnay, E., and Kang, J.-S.: CO₂ transport uncertainties from the uncertainties in meteorological fields, *Geophysical Research Letters*, 38, <https://doi.org/10.1029/2011GL047213>, 2011.

Liu, L. and Greaver, T. L.: A review of nitrogen enrichment effects on three biogenic GHGs: the CO₂ sink may be largely offset by stimulated N₂O and CH₄ emission, *Ecology Letters*, 12, 1103–1117, <https://doi.org/10.1111/j.1461-0248.2009.01351.x>, 2009.

Liu, Z., Liu, Z., Song, T., Gao, W., Wang, Y., Wang, L., Hu, B., Xin, J., and Wang, Y.: Long-term variation in CO₂ emissions with implications for the interannual trend in PM_{2.5} over the last decade in Beijing, China, *Environmental Pollution*, 266, 115014, <https://doi.org/10.1016/j.envpol.2020.115014>, 2020.

Montzka, S. A., Dlugokencky, E. J., and Butler, J. H.: Non-CO₂ greenhouse gases and climate change, *Nature*, 476, 43–50, <https://doi.org/10.1038/nature10322>, 2011.

Siabi, Z., Falahatkar, S., and Alavi, S. J.: Spatial distribution of XCO₂ using OCO-2 data in growing seasons, *Journal of Environmental Management*, 244, 110–118, <https://doi.org/10.1016/j.jenvman.2019.05.049>, 2019.

Wang, Y., Yuan, Q., Li, T., Zhu, L., and Zhang, L.: Estimating daily full-coverage near surface O₃, CO, and NO₂ concentrations at a high spatial resolution over China based on S5P-TROPOMI and GEOS-FP, *ISPRS Journal of Photogrammetry and Remote Sensing*, 175, 311–325, 2021a.

Wang, Y., Yuan, Q., Li, T., and Zhang, L.: Global long-term (2010–2020) daily seamless fused XCO₂ and XCH₄ from CAMS, OCO-2, and GOSAT, <https://doi.org/10.5281/zenodo.7388893>, 2022b.

Yoro, K. O. and Daramola, M. O.: Chapter 1 - CO₂ emission sources, greenhouse gases, and the global warming effect, in: *Advances in Carbon Capture*, edited by: Rahimpour, M. R., Farsi, M., and Makarem, M. A., Woodhead Publishing, 3–28, <https://doi.org/10.1016/B978-0-12-819657-1.00001-3>, 2020.

Zhang, L., Li, T., and Wu, J.: Deriving gapless CO₂ concentrations using a geographically weighted neural network: China, 2014–2020, International Journal of Applied Earth Observation and Geoinformation, 114, 103063, <https://doi.org/10.1016/j.jag.2022.103063>, 2022.

Zhang, M. and Liu, G.: Mapping contiguous XCO₂ by machine learning and analyzing the spatio-temporal variation in China from 2003 to 2019, Science of The Total Environment, 858, 159588, <https://doi.org/10.1016/j.scitotenv.2022.159588>, 2023.

Q1.13: L529: 108 000 European cities.

Response: Thank the referee for his/her comment. The unreadable text of this reference has been revised in the manuscript.

The main revision is as follows:

Moran, D., Pichler, P.-P., Zheng, H., Muri, H., Klenner, J., Kramel, D., Többen, J., Weisz, H., Wiedmann, T., Wyckmans, A., Strømman, A. H., and Gurney, K. R.: Estimating CO₂ emissions for 10000 European cities, Earth System Science Data, 14, 845–864, <https://doi.org/10.5194/essd-14-845-2022>, 2022.

Last but not least, we gratefully thank the referee again for his/her significant comments and suggestions, which have greatly helped us to improve the technical quality and presentation of our manuscript.